



Mice Engrafted with Human Fetal Thymic Tissue and Hematopoietic Stem Cells Develop Pathology Resembling Chronic Graft-versus-Host Disease

Jennifer L. Lockridge¹, Ying Zhou², Yusof A. Becker¹, Shidong Ma³, Shannon C. Kenney³, Peiman Hematti⁴, Christian M. Capitini⁵, William J. Burlingham², Annette Gendron-Fitzpatrick⁶, Jenny E. Gumperz^{1,*}

¹ Department of Medical Microbiology and Immunology, University of Wisconsin School of Medicine and Public Health, Madison, Wisconsin

² Department of Transplantation Surgery, University of Wisconsin School of Medicine and Public Health, Madison, Wisconsin

³ Department of Oncology, University of Wisconsin School of Medicine and Public Health, Madison, Wisconsin

⁴ Department of Medicine and Carbone Cancer Center, University of Wisconsin School of Medicine and Public Health, Madison, Wisconsin

⁵ Department of Pediatrics and Carbone Cancer Center, University of Wisconsin School of Medicine and Public Health, Madison, Wisconsin

⁶ Comparative Pathology Laboratory, Research Animal Resources Center, University of Wisconsin School of Medicine and Public Health, Madison, Wisconsin

Article history:

Received 7 January 2013

Accepted 10 June 2013

Key Words:

Chronic GVHD

Humanized mouse

ABSTRACT

Chronic graft-versus-host disease (cGVHD) is a significant roadblock to long-term hematopoietic stem cell (HSC) transplantation success. Effective treatments for cGVHD have been difficult to develop, in part because of a paucity of animal models that recapitulate the multiorgan pathologies observed in clinical cGVHD. Here we present an analysis of the pathology that occurs in immunodeficient mice engrafted with human fetal HSCs and implanted with fragments of human fetal thymus and liver. Starting at time points generally later than 100 days post-transplantation, the mice developed signs of illness, including multiorgan cellular infiltrates containing human T cells, B cells, and macrophages; fibrosis in sites such as lungs and liver; and thickened skin with alopecia. Experimental manipulations that delayed or reduced the efficiency of the HSC engraftment did not affect the timing or progression of disease manifestations, suggesting that pathology in this model is driven more by factors associated with the engrafted human thymic organoid. Disease progression was typically accompanied by extensive fibrosis and degradation of the thymic organoid, and there was an inverse correlation of disease severity with the frequency of FoxP3⁺ thymocytes. Hence, the human thymic tissue may contribute T cells with pathogenic potential, but the generation of regulatory T cells in the thymic organoid may help to control these cells before pathology resembling cGVHD eventually develops. This model thus provides a new system to investigate disease pathophysiology relating to human thymic events and to evaluate treatment strategies to combat multiorgan fibrotic pathology produced by human immune cells.

© 2013 American Society for Blood and Marrow Transplantation.

INTRODUCTION

Graft-versus-host disease (GVHD) is the major clinical complication of hematopoietic stem cell (HSC) transplantation therapies that are used to treat high-risk hematological malignancies. Because GVHD is associated with significant rates of morbidity and mortality, it is also the major factor preventing the wider application of HSC transplantation to patients with other types of malignancies. Two types of GVHD can develop after HSC transplantation, termed acute (aGVHD) and chronic (cGVHD) [1]. The 2 forms of GVHD typically produce pathology in many of the same tissues, including skin, lung, liver, and eye, and until recently were differentiated mainly by their time of onset (<100 days after transplantation for aGVHD versus longer for cGVHD). However, it is now clear that aGVHD and cGVHD involve sufficiently distinct pathophysiologies that they can be

distinguished by their clinical presentation: aGVHD is characterized by inflammatory processes that include TH1 cytokine production, cytopathic T cell activation, and necrotic damage to target organs, whereas cGVHD appears to be more similar to autoimmune vascular diseases and involves inflammation that leads to fibrotic pathology [1–3]. The development of improved therapeutic strategies is thus likely to require experimental systems that accurately model the distinct clinical manifestations of GVHD.

It is known that aGVHD is mainly due to the transfer of mature T cells from the donor that are not tolerized to the host's antigenic environment, because it is prevented by complete removal of donor T cells from the graft [1]. In contrast, cGVHD is thought to be caused by donor cells that develop de novo within the host from the transplanted HSCs [3]. Cells implicated in cGVHD include T lymphocytes, B lymphocytes, and macrophages; however, the relative contributions of these cell types remain poorly understood. Murine transplantation models have demonstrated that pathology resembling cGVHD can arise through an MHC class II mismatch protocol that leads to B cell overproduction of autoantibodies [4–6], or through a minor histocompatibility mismatch protocol that results in fibrosis associated

Financial disclosure: See Acknowledgments on page 12.

* Correspondence and reprint requests: Jenny E. Gumperz, Department of Medical Microbiology and Immunology, University of Wisconsin School of Medicine and Public Health, 1550 Linden Drive, Madison, WI 53706.

E-mail address: jegumperz@wisc.edu (J.E. Gumperz).

1083-8791/\$ – see front matter © 2013 American Society for Blood and Marrow Transplantation.

<http://dx.doi.org/10.1016/j.bbmt.2013.06.007>

with alternatively activated macrophages [7], or through a protocol that interferes with the negative selection of T cells by MHC class II–expressing dendritic cells in the thymus [8]. In each of these approaches, donor T cells play a central role in disease pathogenesis, but their cellular interactions leading to pathology probably differ markedly. Moreover, although experimental model systems such as these have provided important insights into mechanisms that can lead to cGVHD, the degree to which these systems recapitulate the cGVHD that occurs in humans after HSC transplantation remains a significant concern.

Recently, it has been shown that highly immune-deficient mice that are transplanted with fragments of human fetal thymus and liver along with autologous human fetal HSCs manifest symptoms of GVHD at time points typically >100 days post-transplantation [9]. Thus, this type of model recapitulates a common feature of clinical cGVHD in humans. However, the type of GVHD pathology that occurs in this engraftment model is not yet well characterized. Because the engrafted human T cells in this model mainly seem to mature within a human thymic organoid that develops from the implanted thymic tissue, they may not be effectively tolerized to the xenogeneic environments encountered in the murine host's tissues. The resulting lack of peripheral tolerance might be expected to lead to aGVHD-like pathology. On the other hand, because there is little or no cotransfer of mature T cells along with the graft and the human T cells develop from human precursor populations within the murine host, this model recapitulates human transplantation conditions associated with cGVHD and not aGVHD. Here, we have undertaken an analysis designed to compare the nature of the GVHD pathology that occurs in immunodeficient mice after engraftment of human fetal HSCs, liver, and thymus, with that occurring after transfer of adult human peripheral blood mononuclear cells (PBMCs) containing mature T cells, a protocol that is known to lead to a rapid-onset xenogeneic GVHD response bearing similarity to aGVHD.

METHODS

Generation of Engrafted Mice

All research reported here was performed in accordance with protocols approved by the University of Wisconsin's Institutional Animal Care and Use Committee (IACUC) and Institutional Review Board (IRB). NOD.Cg-Prkdc^{scid} IL2rg^{tm1Wjl}/SzJ mice were obtained from Jackson Laboratory (stock no. 005557; Bar Harbor, ME) and bred and maintained in a specific pathogen-free facility using sterilized cages, bedding, food, and water. Mice used for engraftment were 6 to 8 weeks old and included both males and females.

To generate "PBMC" mice, human PBMCs were isolated from freshly drawn blood of healthy adult donors by Ficoll-Paque density gradient centrifugation (GE Healthcare Life Sciences). Purified PBMCs (1×10^7 per mouse) were injected intravenously using an ocular injection site. For the "HSC-L-T" engraftment protocol, the mice were conditioned with sublethal (2 Gy) whole body irradiation before introduction of human tissues, unless noted otherwise. Human fetal thymus and autologous liver tissues of 14 to 20 weeks of gestational age were obtained from cadaverous sources and processed and stored in X-vivo 15 serum-free culture medium (Lonza Biosciences, Allendale, New Jersey). Thymus and liver tissues were cut into fragments (each approximately 1 mm³), and 1 fragment each of thymus and of liver tissue were surgically implanted next to each other under the capsule of the left kidney. Immediately after this surgery, the mice were given an intravenous (ocular) injection of purified human CD34⁺ HSCs (1 to 4×10^5 cells per mouse, unless otherwise noted) that were obtained from the same fetal liver tissue used for surgical engraftment.

HSCs were prepared by gently disrupting the liver tissue by cutting it into small pieces and repeatedly pipetting up and down and then filtering the resulting cell suspension through a 70- μ m mesh and purifying the mononuclear cells by Ficoll-Paque (GE Healthsciences) density gradient separation. CD34⁺ cells were then purified by magnetic sorting using anti-CD34 microbeads (Miltenyi Biotec, Auburn, CA). The purity of the injected CD34⁺ cells was determined by flow cytometric analysis to typically be at

least 80% to 90%, with less than 0.5% contamination of CD3⁺ cells. The drinking water for the mice was supplemented with 0.17 to 0.25 mg/mL Enrofloxacin (Bayer Healthcare, Leverkusen, Germany) for 14 days after surgery to prevent infections.

Flow Cytometry

Successful engraftment of human cells in the mice was confirmed by flow cytometric analysis of peripheral blood samples. Antibodies used to specifically detect human cells were as follows: pan CD45 (clone HI30), CD4 (clone RPA-T4 or OKT4), CD14 (clone M5E2), CD19 (clone HIB19), and CD3 (clone SPVT-3b). Negative control antibodies used were clone P3 (IgG1) and clone UPC10 (IgG2a). We confirmed that none of these antibodies showed significant staining of murine cells from unengrafted mice (data not shown). For flow cytometric analysis, blood samples were collected into heparinized tubes. The samples were then subjected to ACK lysis to remove red blood cells, blocked with human serum, and stained using 10 μ g/mL of each fluorescently labeled antibody in a PBS buffer containing 1 mg/mL BSA. The samples were analyzed using a flow cytometer (model LSRII; Becton Dickinson, Franklin Lakes, New Jersey), and the data were processed using Flowjo software (Tree Star, Inc.).

Symptom Tracking

Engrafted mice were weighed and evaluated for evidence of symptoms 2 to 3 times each week. Symptom scores were determined blindly, without access to engraftment protocol or prior scoring history. The categories used for scoring were hunching and lethargy, squinting, and alopecia. Alopecia was scored separately for the back, forehead, abdomen, face and nose, and around the eyes. The average of the individual scores for these sites was then taken to generate the total alopecia score. A scale of 0 to 3 was used for each symptom category, according to the following benchmarks:

- *Hunching and lethargy*: 0 = mouse runs around during weighing and is able to extend body fully; 1 = mouse shows little movement in container during weighing; 2 = mouse remains in a curled position during weighing; 3 = spine of mouse is curved and not able to fully straighten
- *Squinting*: 0 = eyes appear round and blinking does not occur more frequently than once every 10 seconds; 1 = eyes are able to open fully but blinking in 1 or both eyes occurs more frequently than once per 10 seconds; 2 = eyes never appear to open all the way; 3 = eyes remain shut during weighing or eyes are partially open and show evidence of crustiness around eyelids or whiteness is visible on cornea
- *Alopecia*: 0 = fur appears of normal density (although some ruffling may be visible); 1 = some evidence of fur thinning; 2 = patches of skin are visible; 3 = skin is exposed and shows evidence of rawness or bleeding

Composite symptom scores were determined by the taking the sum of the squinting, hunching, and average alopecia scores for each mouse. Mice were declared moribund when they were found to have undergone at least 15% loss of body weight or their disease manifestations interfered with their ability to eat or drink as determined by veterinarians blinded to experimental group. Moribund mice were killed by CO₂ inhalation according to IACUC guidelines.

Histology

Tissues were fixed in 10% buffered formalin and embedded in paraffin before sectioning. Sections were deparaffinized and processed for H & E staining or immunohistochemistry. Immunohistochemistry was performed using antibodies against the following human antigens: CD3 or CD45 (Biocare Medical, Concord, CA), CD68 (DAKO, Carpinteria, CA), or CD20 (BD-Pharmingen, Franklin Lakes, NJ). Antigen retrieval was performed using rodent decloaker (Biocare Medical). Antibody labeling was detected and visualized using a horseradish peroxidase–polymer kit with diaminobenzidine development (Biocare Medical). Collagen deposition in tissue sections was visualized using a Gomori 1-step aniline blue trichrome kit (Newcomer Supply, Inc., Middleton, WI) according to the manufacturer's protocol. Histochemically stained tissue sections were analyzed by light microscopy using a Nikon Eclipse microscope (Melville, NY), and color photographic images were acquired using a Spot Insight camera.

Liver Enzyme Quantification

Blood samples collected into heparinized tubes were centrifuged to pellet the cells, and plasma was withdrawn and stored frozen at -20°C until analysis. Plasma samples were analyzed in parallel for aspartate transaminase (AST) and alanine transaminase (ALT) enzyme activity levels using slides (Vitros Chemistry Products) on a Vitros 5,1 FS Chemistry System automated analyzer (Ortho Clinical Diagnostics, Rochester NY).

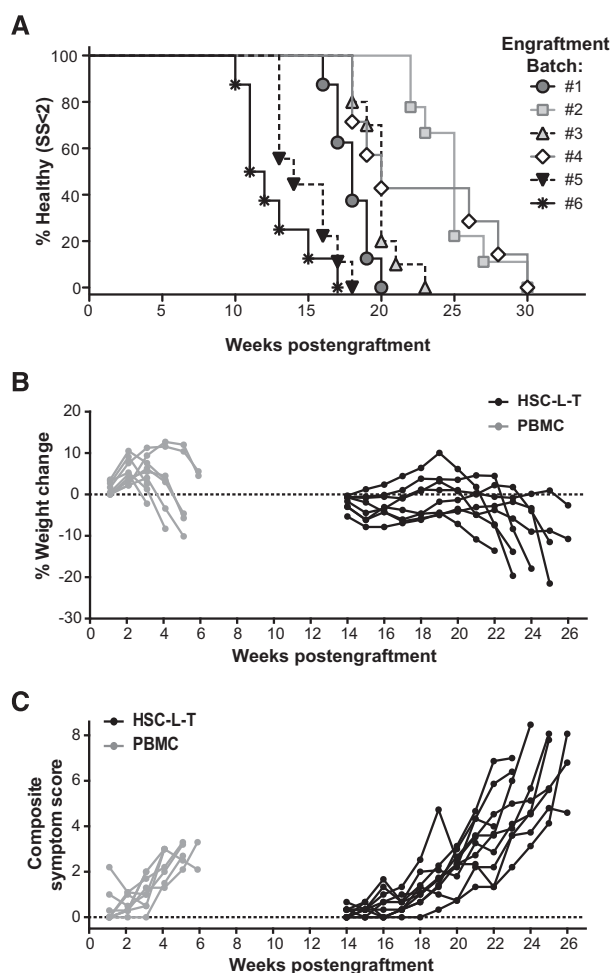


Figure 1. Timing and progression of GVHD in transplanted mice. (A) Plot showing timing of disease onset (defined as a composite symptom score of 2.0 or greater) in 6 different engraftment batches of HSC-L-T mice. The numbers of mice included in each batch are as follows: 8 in batch 1, 9 in batch 2, 13 in batch 3, 12 in batch 4 (3 censored), 9 in batch 5, 9 in batch 6. The survival curves for the batches were significantly different ($P < .0001$, using a log-rank Mantel-Cox test), and median times at onset ranged from 11.0 to 22.3 weeks postengraftment. (B and C) Plots showing progression of weight change and of visible pathology in 9 individual PBMC mice from 4 different engraftment batches (gray symbols) and in 10 individual HSC-L-T mice from batch 3 (black symbols). The plot in B shows the percent weight change over time of each mouse compared with its starting measurement, and the plots in C show the results over time from evaluation of each mouse using a blinded scoring system that generated a composite symptom score on a scale of 0 to 9.

Quantification of Igk

Plasma samples were analyzed for levels of human Igk light chain using a sandwich ELISA. Briefly, high-protein-binding microtiter plates were coated with a capture mAb specific for human Igk light chain (clone MHK-49; Biolegend, San Diego, CA) at a concentration of 2 μ g/mL and then blocked with 10 mg/mL BSA in PBS. Samples included plasma from engrafted mice or human serum as a positive control and were diluted before analysis in medium containing 10% bovine calf serum. Detection was accomplished using a biotinylated version of the same anti-Igk mAb (Biolegend), followed by streptavidin–horseradish peroxidase and visualization using a TMB substrate.

RESULTS

Immunodeficient NOD mice bearing the *Prkdc*^{scid} mutation and having a genetic deletion of the common γ chain of the IL-2 receptor (hereafter called “NSG” mice) were used for engraftment. Two different engraftment models were used. In the first, the mice were subjected to

sublethal total body irradiation, and then fragments of human fetal liver and thymus tissue were surgically implanted under the kidney capsule and autologous human CD34⁺ HSCs were intravenously injected (“HSC-L-T” mice). HSC-L-T mice were generated in batches of 8 to 14 mice engrafted with the same set of autologous human tissues. In the second model, the mice were not irradiated (because we observed in preliminary experiments that total body irradiation of these mice typically led to mortality within 2 weeks after transplantation) and were simply intravenously injected with purified adult human PBMCs (hereafter called “PBMC” mice). For mice engrafted with PBMCs, batches of 3 to 6 mice were injected with cells from a single human donor.

To assess disease onset and progression, the mice were regularly weighed and scored for visible signs of pathology (ie, hunching and lethargy, eye irritation, alopecia). There was no evidence of GVHD in any of the HSC-L-T mice generated in this study for at least 10 weeks, and disease onset typically did not occur until >100 days post-transplantation (Figure 1A). However, the timing of GVHD onset differed significantly ($P < .0001$) among the 6 batches of HSC-L-T mice that we assessed in this analysis, with the median times varying from 11.0 to 22.3 weeks after transplantation (Figure 1A). Near the time of disease onset, the HSC-L-T mice sometimes showed a modest decline in body weight (typically $\leq 10\%$), but weight loss did not become more severe until 8 to 12 weeks later (Figure 1B). They also developed conditions such as blinking or squinting, alopecia, and hunched posture that gradually progressed in severity (Figure 1C). Histological analyses confirmed the presence of inflammatory infiltrates in the eyelids, conjunctiva, and lacrimal glands of mice that showed signs of eye irritation (Table 1), and immunohistochemical analysis demonstrated that the infiltrating cells were largely composed of human T cells (Figure 2B). Similarly, alopecia was associated with marked infiltration of human T cells into the base and shaft of hair follicles (Figure 3B,C).

The PBMC-engrafted mice showed a different pattern of GVHD manifestations. Disease onset occurred within 4 weeks post-transplantation in these mice (Figure 1B and C). Although they typically gained weight in the first 2 weeks, they then generally began to lose weight, becoming moribund within about 6 weeks post-transplantation (Figure 1B). The signs of GVHD observed in these mice were mainly hunching, lethargy, and eye irritation, with little or no alopecia (Figures 2 and 3). Consistent with the low incidence of alopecia, histological and immunohistochemical analyses of the PBMC mice demonstrated that although there was extensive infiltration of the skin by human cells, the infiltration tended to be more confined to dermal rather than epidermal layers, and there was much less evidence of human T cells within hair follicles (Figure 3B and C).

Histopathology of Internal Organs

To further evaluate the GVHD pathology arising in the 2 types of engrafted mice, we performed histological and immunohistochemical analyses of a series of tissues. Whereas there was little evidence of inflammation or pathology in nonsymptomatic HSC-L-T mice, there was substantial cellular infiltration and other signs of pathology in most tissues and organs from both PBMC mice and symptomatic HSC-L-T mice (Table 1). However, there were noticeable differences in the nature of the pathology in HSC-L-T mice compared with PBMC mice.

Table 1

Summary of Results from Necropsy and Histological Analyses of Tissues from Engrafted Mice

	Nonsymptomatic HSC-L-T		Symptomatic HSC-L-T				Symptomatic PBMC			
	Mouse No. 81	Mouse No. 86	Mouse No. 63	Mouse No. 83	Mouse No. 60	Mouse No. 57	Mouse No. 1	Mouse No. 3	Mouse No. 5	Mouse No. 6
Sex	F	M	M	F	M	M	F	F	M	M
Irradiated	Yes	Yes	Yes	Yes	Yes	Yes	No	No	No	No
Days postengraftment at time of analysis	120	120	134	155	128	142	42	35	35	35
Skin										
Epidermal thickening and hyperkeratosis	–	–	+	+	+	+	–	–	–	–
Epidermal or subepidermal cellular infiltration	–	–	+	+	+	+	+	–	–	–
Dermal cellular infiltration	–	–	–	–	+	+	+	+		
Lung										
Peribronchiolar and perivascular infiltration	–	+	+	+	+	+	+	+	+	+
Alveolar interstitial epithelial hyperplasia	–	–	+	+	+	+	+	+	+	+
Type II pneumocytes	–	–	–	–	–	–	–	+	+	+
Liver										
Portal triad infiltration	+	+	+	+	+	+	+	+	+	+
Parenchymal infiltration	–	–	+	+	+	+	+	+	+	+
Macrophage-lymphocyte clusters	–	+	+	+	+	–	–	–	–	–
Bile duct effacement or reduplication	–	–	–	+	–	+	–	–	–	–
Other										
Eye: Conjunctival or lacrimal gland infiltration	–	–	+	+	+	+	–	+	+	+
Nose: Nasal passage, sinus, or olfactory lobe infiltration	+	–	+	+	+	+	+	+	+	+
Ear: Inner or outer ear canal infiltration	+	+	–	+	+	+	+	+	+	+
Tongue: Submucosal infiltration	–	–	–	–	–	–	+	+	+	+
Salivary gland: Atrophy of the submandibular gland	–	–	–	–	–	+	+	+	+	–
Brain: Meningeal infiltration	–	–	–	–	–	–	–	+	+	+
Gastrointestinal tract: Diarrhea	–	–	–	–	–	–	–	–	–	–

In the lungs, HSC-L-T mice showed mainly peribronchiolar and perivascular cellular infiltration with less evidence of inflammation in the smaller airways and alveoli, whereas cellular infiltration was typically extensively present in both peribronchiolar areas and the parenchymal spaces around the alveoli in PBMC mice (Figure 4A). The makeup of the cellular infiltrate in the lungs of HSC-L-T mice consisted of a mixture of human T cells, B cells, and macrophages, whereas in PBMC mice the cellular infiltrate was dominated by human T cells with few B cells and little or no evidence of macrophages (Figure 4B). Additionally, immunohistochemical staining for collagen showed areas of increased collagen deposition, particularly around the bronchioles, in symptomatic compared with nonsymptomatic HSC-L-T mice (Figure 4C). In contrast, despite the widespread inflammation in the lungs of PBMC mice, the

comparatively modest levels of collagen staining suggested little fibrosis (Figure 4C). However, histological analysis suggested proliferation of type II pneumocytes in the alveoli of the PBMC mice, consistent with alveolar insult (Table 1).

The livers of symptomatic HSC-L-T mice and PBMC mice clearly showed inflammatory infiltrates of human leukocytes that were not present in nonsymptomatic engrafted mice (Figure 5A). In both types of symptomatic mice, the cellular infiltrates were present around portal triads and extended into the parenchyma (Figure 5A); however, there were differences in the cellular composition of the infiltrates. In PBMC mice, they were composed mainly of T cells with some B cells but little or no evidence of monocytic cells (Figure 5B). In contrast, in HSC-L-T mice, they prominently included clusters of epithelioid-like macrophages surrounded by T lymphocytes and a few B cells (Figure 5B). HSC-L-T mice

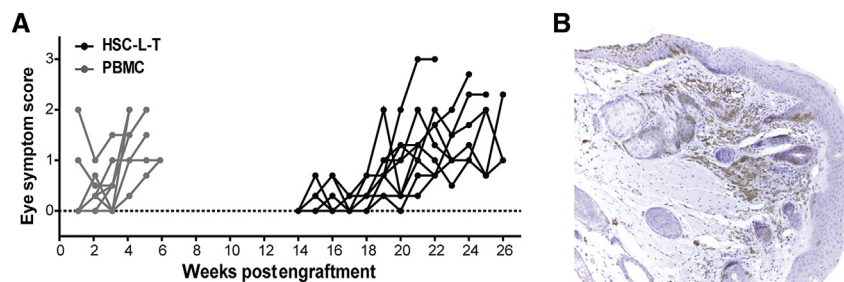


Figure 2. Evaluation of eye irritation. (A) Plot showing the results of a blinded analysis of eye condition over time in 9 individual PBMC mice and 10 individual HSC-L-T mice, using a scale of 0 (no pathology) to 3 (most severe pathology). (B) Immunohistochemical analysis of eyelid tissue for cells expressing human CD3 (brown staining). The tissue was from a symptomatic HSC-L-T mouse at 172 days post-transplantation and was photographed at 20 \times magnification. Similar mononuclear inflammatory infiltrates were observed by histological analysis of H & E–stained tissue (eyelids, conjunctiva, and/or lacrimal glands) from 5 additional HSC-L-T mice and 3 additional PBMC mice.

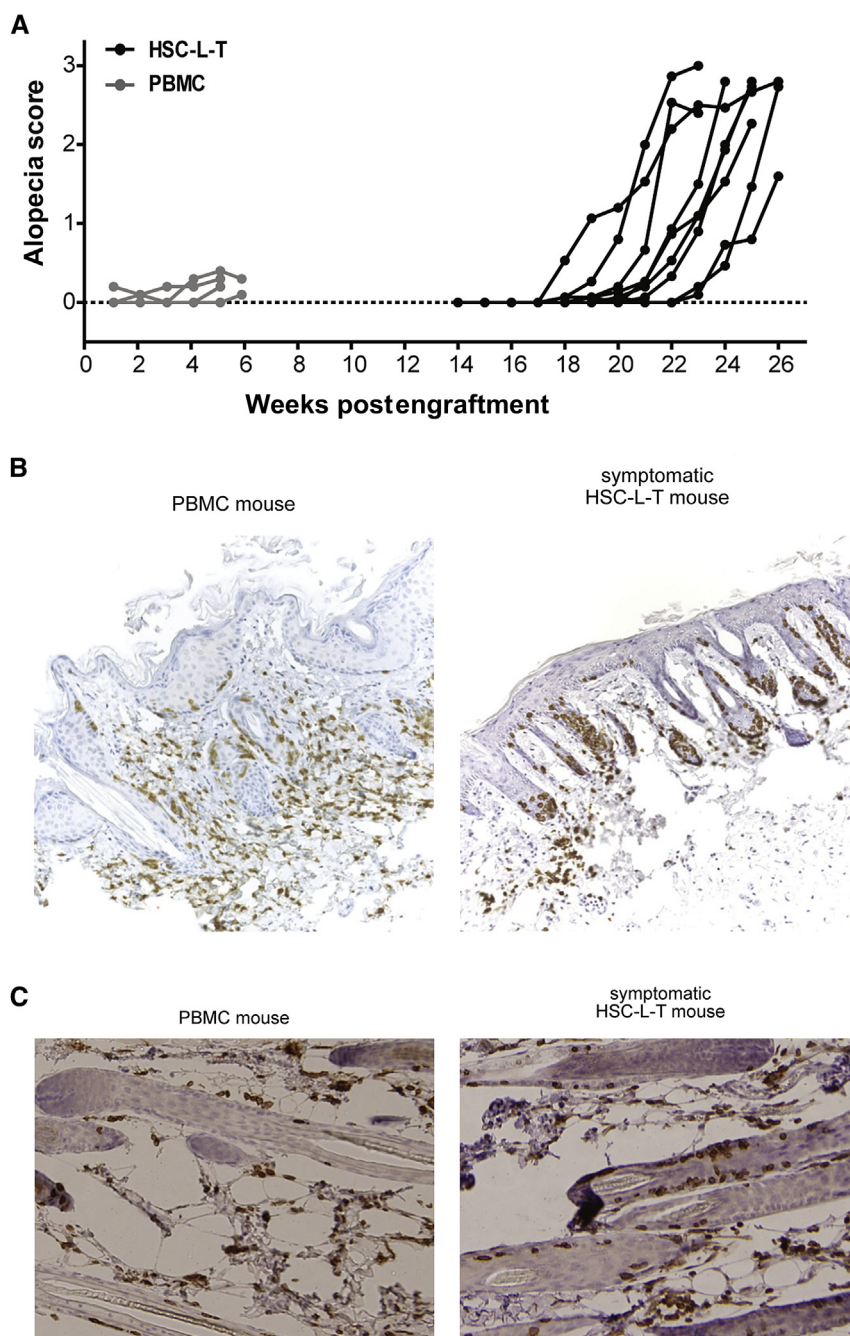


Figure 3. Evaluation of alopecia and skin pathology. (A) Plot showing the results of a blinded analysis of alopecia over time in 9 individual PBMC mice and 10 individual HSC-L-T mice, using a scale of 0 (no pathology) to 3 (most severe pathology). (B and C) Immunohistochemical analyses of skin sections taken from a PBMC mouse at 35 days post-transplantation (left plots) and a symptomatic HSC-L-T mouse at 172 days post-transplantation (right plots) for cells expressing human CD45 (B) or human CD3 (C). Evidence of similar cellular infiltration and localization was observed by histological analysis of H & E–stained skin sections from 7 additional HSC-L-T mice and 3 additional PBMC mice.

sometimes also showed evidence of bile duct effacement, whereas this was not observed in PBMC mice (Table 1). Additionally, collagen staining in the liver was dramatically increased in symptomatic HSC-L-T mice compared with nonsymptomatic mice (Figure 5C), suggesting a highly fibrotic pathology. Symptomatic PBMC mice showed less collagen staining in the liver than symptomatic HSC-L-T mice (Figure 5C), suggesting the inflammatory pathology in these mice was not as highly fibrotic.

Analysis of the levels of transaminase enzyme activity in blood plasma samples from the engrafted mice provided

further evidence of differences in liver pathology. We tested for enzyme activity levels of AST, which is released from liver as well as other tissues upon cellular damage, and also of ALT, which is produced only by hepatocytes and thus more specifically indicates damage to the liver. Compared with nonsymptomatic HSC-L-T mice, plasma samples from symptomatic HSC-L-T mice had slightly elevated activity levels of AST and ALT (Figure 6), although the differences were not statistically significant. In contrast, plasma samples from PBMC mice had approximately 5-fold greater AST and 10-fold greater ALT enzyme activity levels than the

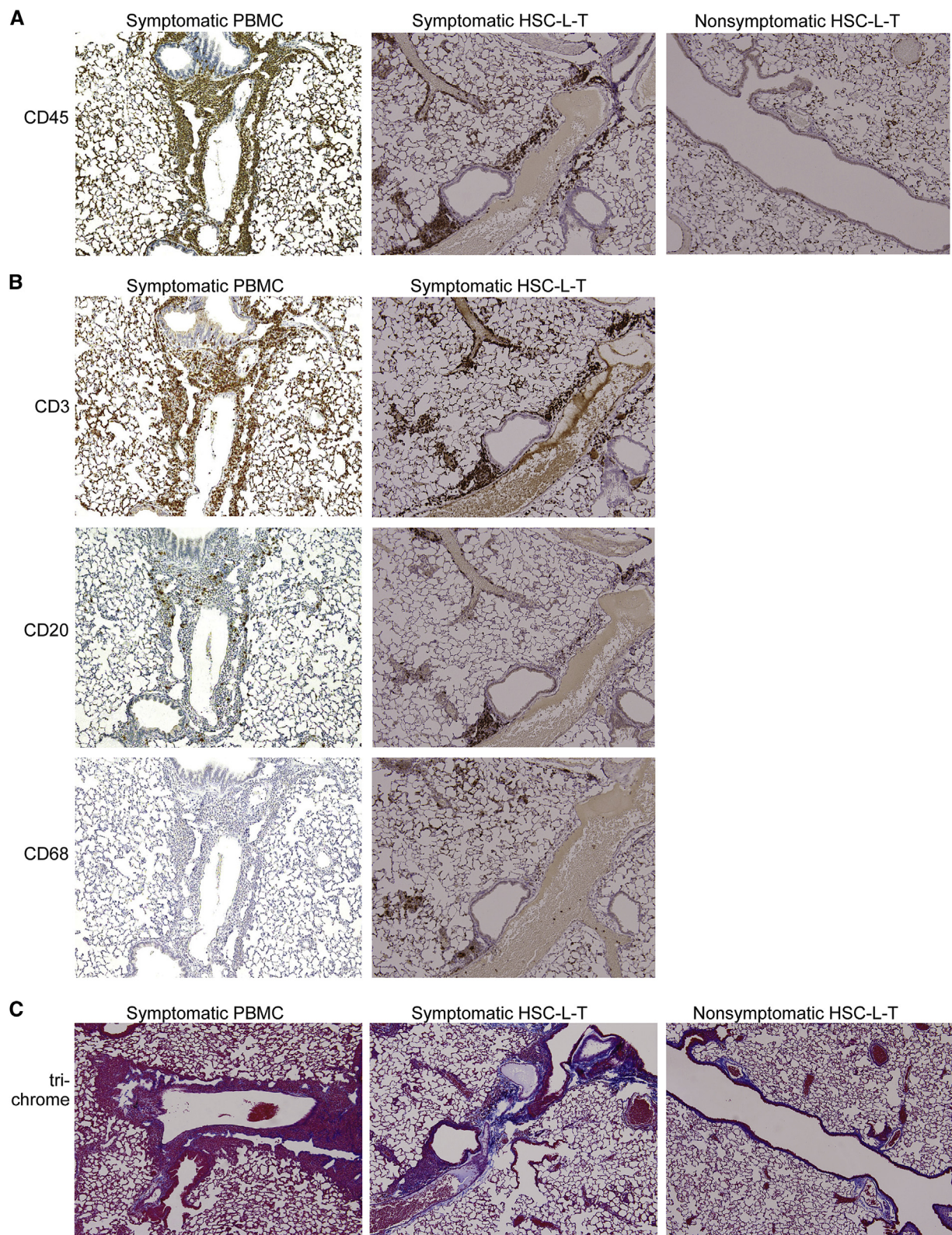


Figure 4. Lung inflammation. (A) Lung tissue sections taken from a PBMC mouse at 35 days post-transplantation, a symptomatic HSC-L-T mouse at 142 days post-transplantation, and a nonsymptomatic HSC-L-T mouse at 120 days post-transplantation were fixed and stained for cells expressing the human CD45 marker (visualized by brown coloration) to detect the presence of human leukocytes. (B) Immunohistochemical staining of serial sections of lung tissue from the same mice shown in A for cells expressing the human CD3, CD20, or CD68 markers (all visualized by brown coloration) to detect T cells, B cells, or macrophages, respectively. (C) Gomori trichrome staining of lung tissue sections from the same mice to detect collagen depositions. Bright blue color indicates collagen fibers; red or pink coloration indicates keratin or muscle fibers or cytoplasm of cells. Photographs in all panels were taken at 10 × magnification. Similar immunohistochemical results were observed for 4 HSC-L-T mice, and evidence of similar cellular infiltration and localization was observed by histological analysis of H & E–stained skin sections from 7 additional HSC-L-T mice and 3 additional PBMC mice.

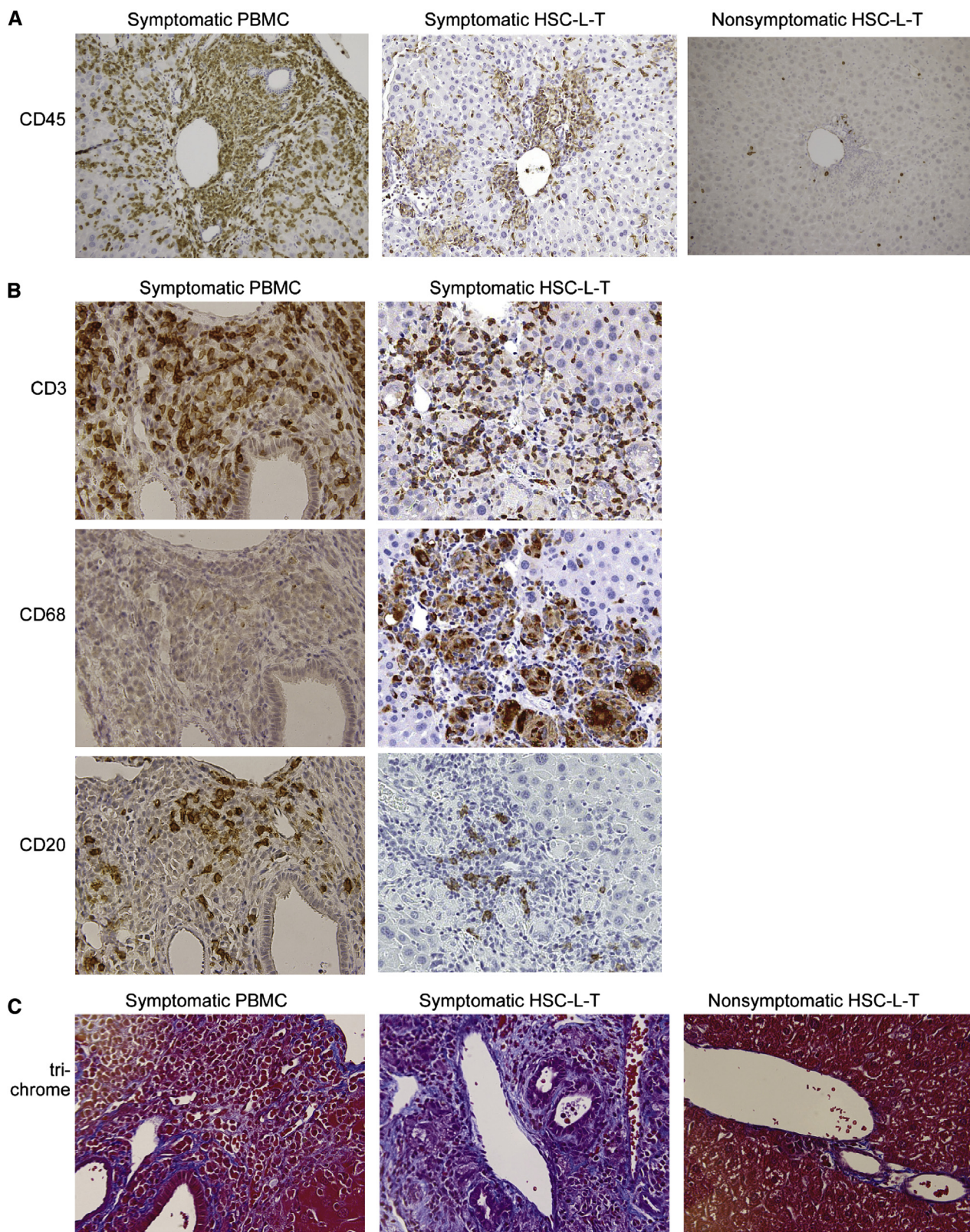


Figure 5. Liver inflammation. (A) Liver tissue sections taken from a PBMC mouse at 35 days post-transplantation, a symptomatic HSC-L-T mouse at 134 days post-transplantation, and a non symptomatic HSC-L-T mouse at 228 days post-transplantation were fixed and stained for cells expressing the human CD45 marker (brown color). Photographs were taken at 20 \times magnification. (B) Sections of liver tissue from the mice shown in A were stained for cells expressing the human CD3, CD20, or CD68 markers (brown color). Images are shown at 40 \times magnification. (C) Gomori trichrome staining showing collagen deposition (blue color) in liver tissue sections from the indicated mice. Images are shown at 40 \times magnification. Similar immunohistochemical results were observed for 4 HSC-L-T mice, and evidence of similar cellular infiltration and localization was observed by histological analysis of H & E-stained skin sections from 7 additional HSC-L-T mice and 3 additional PBMC mice.

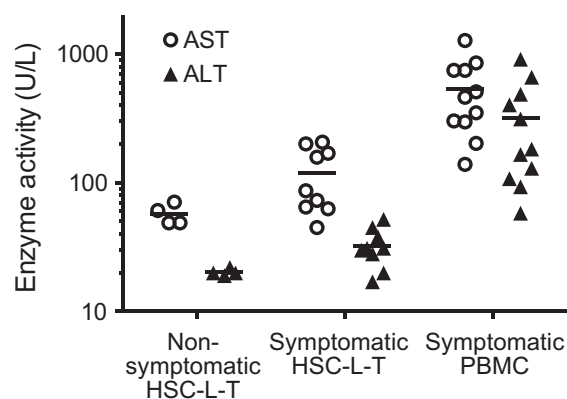


Figure 6. Transaminase enzyme activity in the plasma of transplanted mice. Plasma samples from the indicated types of engrafted mice were tested for activity levels of the transaminase enzymes AST (open circles) and ALT (filled triangles). Each symbol represents the result from an individual engrafted mouse. Nonsymptomatic HSC-L-T mice were 15 weeks postengraftment at the time of analysis; symptomatic HSC-L-T mice were 19 to 40 weeks post-engraftment; PBMC mice were 3 to 7 weeks postengraftment. AST and ALT enzyme activity values were not significantly different for nonsymptomatic and symptomatic HSC-L-T mice, but were significantly different for symptomatic HSC-L-T mice versus PBMC mice ($P < .001$ for both) using a 2-tailed Mann-Whitney test.

symptomatic HSC-L-T mice (Figure 6), with the differences that appeared to be statistically significant in both cases ($P < .001$, using a 2-tailed Mann-Whitney test). These results thus support the presence of a more acute hepatitis in the PBMC mice, whereas the lower serum transaminase enzyme activity and greater evidence of fibrosis in the symptomatic HSC-L-T mice are more consistent with what is observed clinically in cGVHD patients [10].

Both types of mice frequently showed histological evidence of inflammatory cellular infiltration in the nasal passages, including sinuses and olfactory lobes, and in the inner and outer ear canals (Table 1). Occasionally, inflammatory infiltrates were also observed in teeth, genitalia, and stomach, although neither the HSC-L-T nor the PBMC mice showed evidence of diarrhea (Table 1). Notably, PBMC mice usually also had marked cellular infiltrates in the submucosal layers of the tongue, atrophy of the submandibular salivary glands, and substantial evidence of meningeal infiltration in the brain, whereas these sites rarely appeared to be affected in the HSC-L-T mice (Table 1). Thus, although both types of mice showed histopathology at multiple tissue and organ sites, the affected tissues were somewhat more restricted in the HSC-L-T mice as compared with the PBMC mice, and the nature of the inflammatory infiltrates differed, with more evidence of macrophages and fibrotic processes in the HSC-L-T mice.

Role of HSC versus Thymic Organoid Engraftment

Development of GVHD symptoms has not been reported in immunodeficient mice that receive human HSCs without concurrent implantation of thymic and liver tissue, and hence it seems likely that the GVHD that develops in the HSC-L-T model requires the presence of the human thymic organoid, which promotes T cell engraftment [11]. Although it is clear that long-term engraftment by human T cells requires both the sustained survival of the thymic organoid and bone marrow engraftment of human HSCs [12], the relative importance of the thymic tissue versus the HSCs to the development of GVHD is not clear. To investigate this, we

generated HSC-L-T mice that were all implanted with similar sizes of human thymic and liver fragments but were administered different doses of HSCs. Mice that received the lowest dose of HSCs (1×10^4 cells per mouse) showed delayed emergence of human leukocytes in the periphery but eventually developed levels of engraftment similar to mice that received higher doses of HSCs (1×10^5 or 2×10^5 cells per mouse) (Figure 7A). In the mice that received the lowest HSC dose, the human leukocyte population was initially highly skewed toward T cells with only very low frequencies of B cells, but over time the lymphocyte proportions became similar to those of mice that were administered higher doses of HSCs (Figure 7A). Remarkably, the reduced dose of HSCs had no impact on the time of GVHD symptom onset, rate of symptom progression, or degree of symptom severity (Figure 7B). These results suggested that the development of GVHD in this model is not highly dependent on the rate of HSC engraftment.

To further investigate, we compared mice that were irradiated before engraftment with mice that had not been irradiated. Irradiation not only suppresses host immune responses that might attack the engrafted cells, it also directly facilitates engraftment of HSCs by making space in the bone marrow. Therefore, non-irradiated mice should have diminished or delayed HSC engraftment, but there should be little or no impact on the engraftment of the thymic organoid. Interestingly, there was no difference between irradiated and non-irradiated mice in the timing of GVHD onset, and the non-irradiated mice showed similarly widespread histopathology as the irradiated mice (Figure 7C and Table 2). The non-irradiated and irradiated mice had comparable levels of T cells, but the irradiated mice had much lower levels of circulating B cells (mean of .2% of the PBMC for irradiated versus 9.4% for non-irradiated) (Figure 7D). Notably, despite the very low B cell frequencies in non-irradiated mice, we found that these mice had clearly detectable human immunoglobulin in their plasma and that their levels of immunoglobulin increased to nearly the same levels as irradiated mice at late time points after transplantation (Figure 7E). Thus, although efficient B cell reconstitution does not seem to be required for the development of GVHD in this model, there may nevertheless be a role for B cell activation during disease progression. However, because the efficiency of HSC engraftment and B cell reconstitution did not produce a marked effect on GVHD disease onset, these results directed our attention to the human thymic organoid.

Thymic Organoid Histopathology

Histological analyses of the engrafted kidneys of HSC-L-T mice with moderate or severe GVHD symptoms consistently revealed extensive fibrosis at the border between the kidney and the thymic organoid and structural degradation of the organoid itself, whereas the engrafted kidneys and thymic organoids of nonsymptomatic mice typically appeared to be healthy (Figure 8A). We also found that cells staining strongly for the Forkhead box P3 transcription factor (FoxP3), a marker of regulatory T cells (Tregs), were present in the medullary areas of thymic organoids from nonsymptomatic HSC-L-T mice (Figure 8B, left). In contrast, there was little evidence of cells staining strongly for FoxP3 in thymic organoids from mice with severe GVHD symptoms (Figure 8B, right). A blinded quantitation of the number of FoxP3⁺ cells per field in a series of slides from mice with varying GVHD symptom scores revealed an inverse

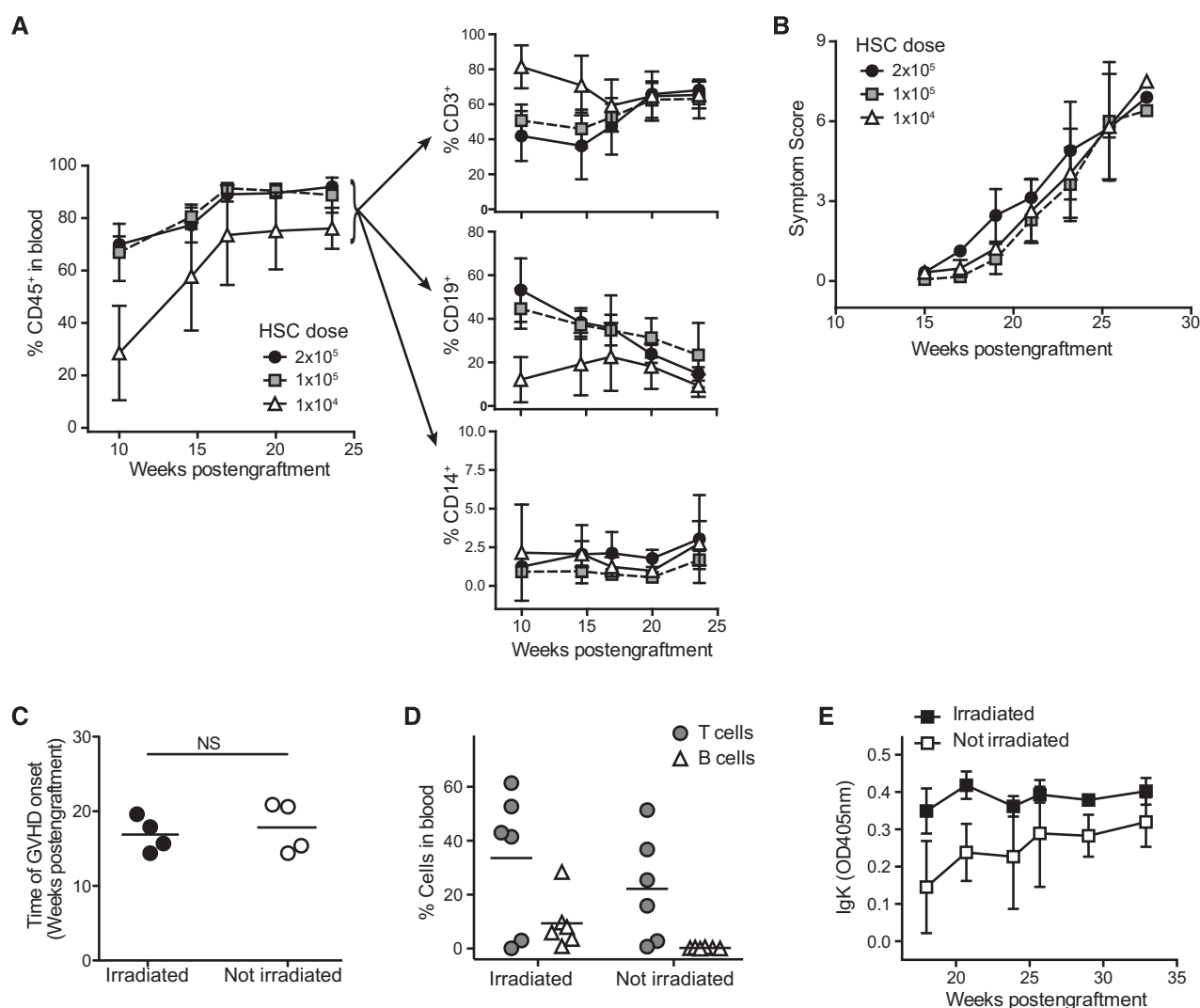


Figure 7. The impact of modulating HSC engraftment on the development of GVHD. (A) An engraftment batch of HSC-L-T mice was divided into 3 groups (4 to 6 mice in each) that were all implanted with similar-sized fragments of human fetal thymus and liver tissue, and each group was administered a different dose of purified human CD34⁺ HSCs. The plot on the left shows the mean frequencies of cells in the blood expressing the human CD45 marker, as determined by flow cytometric analysis. Plots on the right show the mean percentages of the human CD45⁺ cells that expressed CD3 (T cells), CD19 (B cells), or CD14 (monocytes). Error bars show the standard deviations of the means. (B) Plot showing composite GVHD symptom score over time for each group of mice shown in A as determined by a blinded analysis. (C) Mice were either subjected to sublethal irradiation or not irradiated before implantation of human fetal thymus and liver fragments and administration of purified human CD34⁺ HSCs (1×10^5 per mouse). The plot shows the time of GVHD symptom onset for individual mice in each group. The 2 groups were not significantly different. (D) Frequencies of cells expressing human CD3 (T cells) or human CD19 (B cells) in the peripheral blood of individual mice in the 2 groups at 15 weeks postgraftment. T cell frequencies were not significantly different for the 2 groups, but the B cell frequencies showed a significant difference ($P = .0022$), using a 2-tailed Mann-Whitney test. (E) The amount of circulating human IgK light chain was estimated by using a sandwich ELISA to test plasma samples drawn from irradiated and non-irradiated mice at the indicated times after engraftment. The plot shows the mean optical density values obtained from samples from 4 irradiated and 3 non-irradiated mice, with error bars indicating the standard deviations of the means.

correlation of FoxP3⁺ thymocytes with disease severity (Figure 8C). Together, these observations further underscore an association between the biological properties of the engrafted human thymic organoid and the development of GVHD pathology in the HSC-L-T model.

DISCUSSION

The results presented here demonstrate for the first time that immune-deficient mice administered human fetal HSCs and concurrently implanted with fragments of human fetal thymus and liver go on to develop pathologies that resemble cGVHD. Specifically, we show that the HSC-L-T mouse engraftment model recapitulates a number of features of cGVHD observed in human HSC transplantation patients.

First, GVHD symptoms did not typically appear in HSC-L-T mice until >100 days post-transplantation, similar to the timing at which cGVHD tends to occur in human patients [2]. Second, human patients with cGVHD frequently have alopecia (hair loss) and scleroderma-like pathology, a condition characterized by chronic inflammation and fibrosis in which the skin becomes thickened with reduced elasticity [13]. In the HSC-L-T mouse model, the skin became thickened and tight with restricted flexibility, there was often significant alopecia, and there was evidence of extensive infiltration of the epidermal layers by human hematopoietic cell types. Third, lung involvement in human patients with cGVHD generally manifests as constricted breathing resulting from inflammation around the bronchioles and fibrosis

Table 2
Summary of Histopathology Observed in Irradiated versus Non-Irradiated HSC-L-T Mice

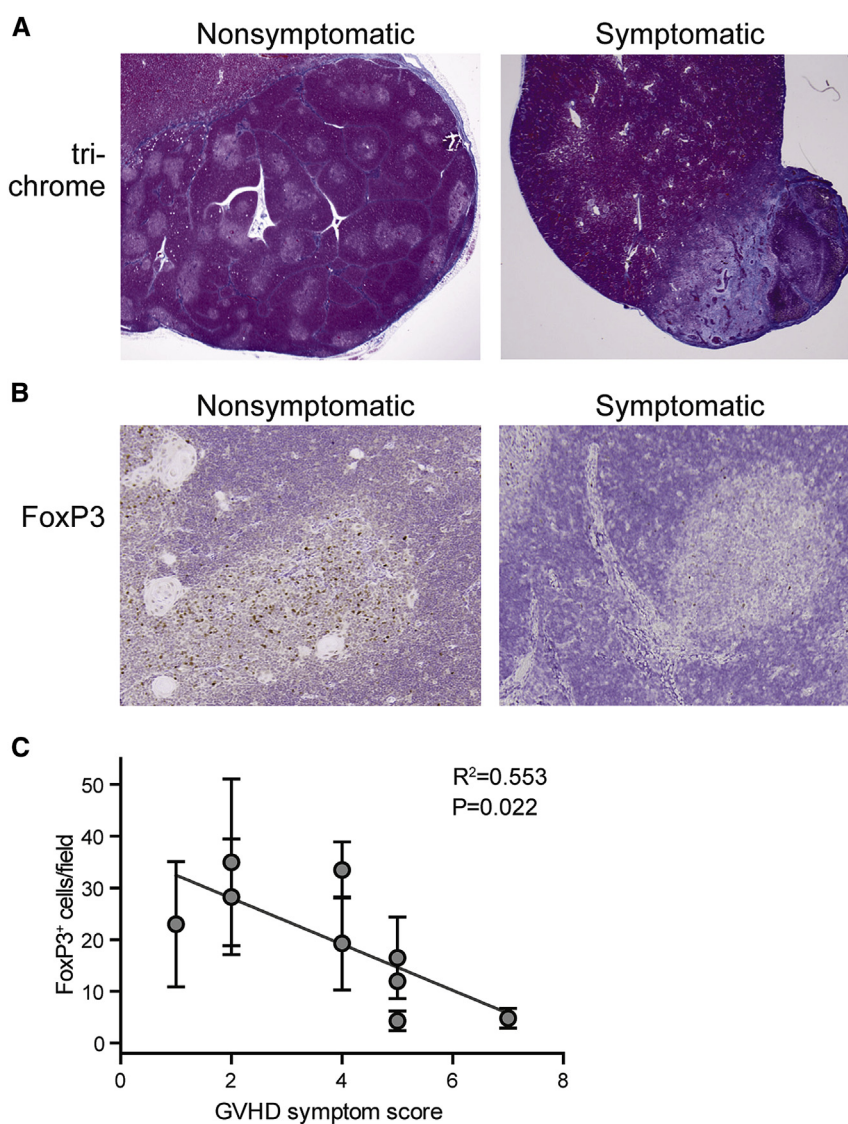
	Irradiated HSC-L-T			Non-Irradiated HSC-L-T				
	Mouse No. 63	Mouse No. 83	Mouse No. 60	Mouse No. 57	Mouse No. 64	Mouse No. 67	Mouse No. 69	Mouse No. 71
Sex	M	F	M	M	M	M	M	M
Irradiated	Yes	Yes	Yes	Yes	No	No	No	No
Days postengraftment at time of analysis	134	155	128	142	142	128	209	217
Skin								
Epidermal thickening and hyperkeratosis	+	+	+	+	+	+	+	+
Epidermal or subepidermal cellular infiltration	+	+	+	+	+	+	+	+
Dermal cellular infiltration	–	+	–	–	+	–	+	–
Lung								
Peribronchiolar and perivascular infiltration	+	+	+	+	+	+	+	+
Alveolar interstitial epithelial hyperplasia	+	+	+	+	+	+	+	+
Type II pneumocytes	–	–	–	–	–	+	+	+
Liver								
Portal triad infiltration	+	+	+	+	+	+	+	+
Parenchymal infiltration	+	+	+	+	+	+	+	+
Macrophage-lymphocyte clusters	+	+	+	+	+	+	+	+
Bile duct effacement or reduplication	–	+	–	+	+	+	–	–
Other								
Eye: Conjunctival or lacrimal gland infiltration	+	+	+	+	+	–	+	+
Nose: Nasal passage, sinus, or olfactory lobe infiltration	+	+	+	+	–	–	–	–
Ear: Inner or outer ear canal infiltration	–	+	+	+	+	+	+	+
Tongue: Submucosal infiltration	–	–	–	–	–	+	–	+
Salivary gland: Atrophy of the submandibular gland	–	–	–	+	–	+	–	–
Brain: Meningeal infiltration	–	–	–	–	–	–	–	–
Gastrointestinal tract: Diarrhea	–	–	–	–	–	–	–	–

or occlusion of the airways (obliterative bronchiolitis) [14]. We found that the lungs of HSC-L-T mice showed cellular infiltration mainly around the bronchioles, with less infiltration in the parenchymal spaces around the alveoli, and there appeared to be an excess of collagen deposited around the bronchiolar passages. Fourth, liver pathology observed in cGVHD patients typically entails bile duct inflammation, leading to cholestasis and fibrotic damage [10,15]. The livers of symptomatic HSC-L-T mice consistently had substantial cellular infiltrates around the portal triads and sometimes showed evidence of bile duct effacement. Histological and immunohistochemical analyses of the inflammatory infiltrates revealed prominent granulomatous aggregates containing epithelioid-like macrophages, which are often associated with fibrosis. Moreover, histological staining for collagen deposition suggested substantial fibrosis of the liver tissue. Analysis of plasma samples for liver transaminase enzyme activity suggested liver damage in the HSC-L-T mice, although not as acute as that observed in the PBMC model. Thus, liver pathology in the HSC-L-T mice resembled that observed in cGVHD patients in that it included substantial fibrosis and appeared to have a chronic rather than acute inflammatory profile. Finally, dry eye syndrome is also often associated with cGVHD in human transplantation patients [16]. This syndrome is caused by inflammation of the conjunctiva or cornea and is often associated with impairments in tear production and distribution and accompanied by symptoms of eye irritation, itching, and sensitivity to light. Resembling this, we noted that the HSC-L-T mice usually developed symptoms of squinting and showed histological and immunohistochemical evidence of immune cells infiltrating the eyelids, conjunctiva, and/or lacrimal glands. Thus, in contrast to the GVHD that develops in NSG mice after transplantation of adult human PBMCs, which has more aGVHD-like characteristics, the HSC-L-T model produces multiorgan fibrotic pathologies more similar to cGVHD.

It is also interesting that the nature of the GVHD pathology we observed in the HSC-L-T model more closely

resembles sclerodermatous cGVHD rather than the systemic lupus erythematosus–like manifestations observed in some murine-into-murine models of cGVHD [3]. Sclerodermatous cGVHD pathology arises in murine models in which mature T cells are transplanted from a minor histocompatibility antigen mismatched donor and in models in which thymic negative selection is impaired in the host after transplantation [3]. Our observation that experimental manipulations that impacted the efficiency of HSC engraftment had little or no detectable effect on GVHD onset or progression suggests that processes involving the engrafted human thymic organoid may be the dominant drivers of pathology in the HSC-L-T model. Consistent with this, we found that in NSG mice that receive human HSCs alone (with no thymic graft), there is little or no evidence of GVHD for at least 6 months after transplantation (data not shown). Thus, it seems reasonable to speculate that the high efficiency and long-lasting nature of human T cell engraftment conferred by the coengrafted human thymic organoid may promote the development of GVHD in HSC-L-T mice.

Importantly, the thymic organoid in this model includes human thymic epithelial cells as well as dendritic cells [17,18], which are the cell types known to be responsible for positive and negative selection of developing T cells. Thus, it seems likely that T cells developing in the engrafted human thymic organoid encounter human antigen-presenting molecules upon which they may undergo positive and negative selection. Successful positive selection of developing T cells on these antigen-presenting molecules would facilitate their subsequent ability to interact productively with human antigen-presenting cells that develop from the engrafted HSCs, such as macrophages and B cells. However, if the human thymic organoid provides an environment in which mainly peptides of human origin are involved in negative selection, this step might fail to remove T cells that can recognize murine peptides. A failure to tolerize the human T cell repertoire against murine peptides might result in the pathogenic activation of human T cells by human



print & web 4C/FPO

Figure 8. Integrity of the human thymic organoid after development of GVHD. (A) Gomori trichrome staining of a section of the engrafted kidney of a non-symptomatic mouse at 120 days post-transplantation and a symptomatic mouse at 134 days post-transplantation. The collagen staining (blue color) indicates extensive fibrosis at the border between the thymic organoid and the kidney in the symptomatic mouse, but much less in the nonsymptomatic mouse. Images are shown at $2\times$ magnification and are representative of 2 different mice each. Additional evidence of variable amounts of fibrosis of the thymic organoid that seemed to correlate with GVHD status was observed from analysis of H & E-stained tissues from 8 symptomatic and 3 nonsymptomatic HSC-L-T mice. (B) Immunohistochemical analysis of human thymic organoid sections from a nonsymptomatic mouse at 120 days post-transplantation compared with a symptomatic mouse at 134 days post-transplantation for cells expressing FoxP3 (brown color). Images are shown at $20\times$ magnification. (C) Compiled results of a blinded analysis of the frequency of cells staining positively for FoxP3 in a thymic organoid tissue section (as shown in B) in relation to the GVHD symptom score of the mouse.

antigen-presenting cells in the periphery that have ingested murine proteins and are thus presenting murine peptides on their MHC molecules. It is also possible that the selection processes in the human thymic organoid might fail to efficiently remove T cells that can xenogeneically cross-react on murine antigen-presenting molecules, and that such T cells might therefore become directly activated by host cells encountered in the periphery. In either case, it seems plausible that the similarity of this HSC-L-T model to murine models of sclerodermatous cGVHD results from a failure to properly tolerize the T cell repertoire during negative selection in the engrafted thymic organoid.

Consistent with observations that cGVHD in humans is associated with impairments in thymic function [19–21], we also noted that HSC-L-T mice with GVHD showed structural effacement of the engrafted thymic organoid, whereas the

engrafted thymic tissue appeared healthy in mice that did not develop GVHD symptoms. Although it is not clear from this type of observation whether thymic damage is a cause or an effect of GVHD pathology, it is noteworthy that the severity of GVHD symptoms in the HSC-L-T mice correlated inversely with the frequency of FoxP3⁺ T cells among the medullary thymocytes. It is thus tempting to speculate that Tregs that are generated in the human thymic organoid may serve to limit the pathogenic activities of other T cells in the periphery. In this scenario, a reduction in the frequency of Tregs that is associated with degradation of the thymic organoid might serve to "release" pathogenic T cells in the periphery from inhibition, leading to further GVHD pathology. Notably, 2 studies using similar HSC-L-T models demonstrated the suppressive functions of human Tregs in the peripheral tissues of engrafted mice [22,23], supporting

the possibility that the presence of Tregs produced by functioning human thymic tissue helps to prevent GVHD. Lower levels of Tregs have also been found in HSCT patients with severe cGVHD [24], supporting the idea that these cells may be involved in preventing pathogenesis in clinical settings.

In this regard, it is also worth considering the role of the human fetal liver tissue that is implanted next to the thymic tissue in the HSC-L-T model. Fetal liver tissue has historically been included in most protocols that engraft human thymic tissue into immune-deficient mice [11], because it appears to promote the engraftment and survival of the thymic organoid. However, in addition to CD34⁺ HSCs, the fetal liver tissue that we use contains mature T cells and probably also other cell types such as mesenchymal cells that may influence the development of GVHD. Indeed, although we have not conducted a side-by-side controlled analysis, we observed that signs of GVHD developed remarkably early (approximately 8 weeks postengraftment) in a group of 7 mice transplanted with HSCs and thymic tissue without the fetal liver fragment (data not shown). Thus, the fetal liver tissue may help to delay the onset of GVHD, either by prolonging the survival of the thymic organoid and thus the thymic production of Tregs, or by contributing other regulatory cell types.

The role of B cells in the development of GVHD in the HSC-L-T model also remains unclear. A recent analysis in a murine-into-murine model of allogeneic HSC transplantation resulting in cGVHD, which produces multiorgan pathologies with similarities to those seen here, suggests an important role for B cells and alloantibody deposition, in addition to the actions of CD4⁺ T cells [25]. Given that B cells were clearly detected in inflammatory infiltrates in symptomatic mice, it is reasonable to conclude they are involved in the disease pathophysiology. However, because mice that were not conditioned by sublethal irradiation before engraftment showed highly impaired B cell development yet went on to develop GVHD similarly to mice that had normal B cell engraftment, it seems that efficient B cell engraftment is not required for GVHD onset in this model. Thus, we conclude that B cells may contribute to disease pathology and progression, although they may not be the most important disease initiators. This is consistent with our observation that even in engrafted mice that have very low frequencies of B cells, the circulating human immunoglobulin levels rise at late time points after transplantation, suggesting progressive activation of those B cells that are present. However, to understand the role of B cells in this model, it will be critical to evaluate the extent to which the secreted human immunoglobulin reacts with murine tissue antigens.

Taken together, the results presented here demonstrate that the HSC-L-T model provides a sophisticated experimental system to investigate multiorgan fibrotic pathologies resulting from engraftment of human immune cells. It is important to note that because of significant divergences between this experimental model and clinical HSC transplantation protocols (eg, the cotransplantation of thymus and liver tissue) as well as the xenogeneic nature of this system, it is not necessarily an accurate representation of what happens clinically in humans during cGVHD. However, this model provides a unique opportunity to evaluate preventative and therapeutic treatments for cGVHD in the context of human immune reconstitution, which may be important because human immune cells differ in multiple ways compared with their murine counterparts.

A particular strength is that due to its inclusion of human thymic tissue, this model will allow the exploration of methods to enhance thymopoiesis or thymic functioning and studies aimed at dissecting how thymic events are connected to peripheral pathology. In addition, future studies could be targeted at understanding graft-versus-leukemia effects in the setting of cGVHD, because human leukemia cell lines or primary samples could be concurrently implanted. Finally, the results presented here show there is a substantial window of time after the transplanted human immune cells have developed within the murine host in which there is little or no xenopathology. Thus, the knowledge that GVHD develops in HSC-L-T mice only after a substantial time delay will further facilitate the use of this model for studying immune responses by human cells in the context of many other diseases, including infection by human-specific pathogens such as HIV and EBV.

ACKNOWLEDGMENTS

Financial disclosure: Supported by National Institutes of Health grant R21 AI093935 (to J.E.G.) and grants R01 AI066219 and 1P01 AI084853 (to W.J.B.), and by a grant from the University of Wisconsin Carbone Cancer Center (to J.E.G.).

Conflict of interest statement: C.M.C. was supported by Hyundai Hope on Wheels and the Midwest Athletes Against Childhood Cancer fund. No author has any direct financial interests to declare.

REFERENCES

- Blazar BR, Murphy WJ, Abedi M. Advances in graft-versus-host disease biology and therapy. *Nat Rev Immunol*. 2012;12:443–458.
- Filipovich AH, Weisdorf D, Pavletic S, et al. National Institutes of Health consensus development project on criteria for clinical trials in chronic graft-versus-host disease. I. Diagnosis and staging working group report. *Biol Blood Marrow Transplant*. 2005;11:945–956.
- Chu YW, Gress RE. Murine models of chronic graft-versus-host disease: Insights and unresolved issues. *Biol Blood Marrow Transplant*. 2008;14:365–378.
- Morris SC, Cheek RL, Cohen PL, Eisenberg RA. Autoantibodies in chronic graft versus host result from cognate T-B interactions. *J Exp Med*. 1990;171:503–517.
- Morris SC, Cheek RL, Cohen PL, Eisenberg RA. Allotype-specific immunoregulation of autoantibody production by host B cells in chronic graft-versus host disease. *J Immunol*. 1990;144:916–922.
- Morris SC, Cohen PL, Eisenberg RA. Experimental induction of systemic lupus erythematosus by recognition of foreign Ia. *Clin Immunol Immunopathol*. 1990;57:263–273.
- Jaffee BD, Claman HN. Chronic graft-versus-host disease (GVHD) as a model for scleroderma. I. Description of model systems. *Cell Immunol*. 1983;77:1–12.
- Sakoda Y, Hashimoto D, Asakura S, et al. Donor-derived thymic-dependent T cells cause chronic graft-versus-host disease. *Blood*. 2007;109:1756–1764.
- Greenblatt MB, Vranac V, Tivey T, et al. Graft versus host disease in the bone marrow, liver and thymus humanized mouse model. *PLoS ONE*. 2012;7:e44664.
- Shulman HM, Kleiner D, Lee SJ, et al. Histopathologic diagnosis of chronic graft-versus-host disease: National Institutes of Health Consensus Development Project on Criteria for Clinical Trials in Chronic Graft-versus-Host Disease. II. Pathology Working Group Report. *Biol Blood Marrow Transplant*. 2006;12:31–47.
- McCune JM, Namikawa R, Kaneshima H, et al. The SCID-hu mouse: Murine model for the analysis of human hematolymphoid differentiation and function. *Science*. 1988;241:1632–1639.
- Zhang L, Su L. HIV-1 immunopathogenesis in humanized mouse models. *Cell Mol Immunol*. 2012;9:237–244.
- White JM, Creamer D, du Vivier AW, et al. Sclerodermitous graft-versus-host disease: Clinical spectrum and therapeutic challenges. *Br J Dermatol*. 2007;156:1032–1038.
- Bacigalupo A, Chien J, Barisione G, Pavletic S. Late pulmonary complications after allogeneic hematopoietic stem cell transplantation: Diagnosis, monitoring, prevention, and treatment. *Semin Hematol*. 2012;49:15–24.
- McDonald GB. Hepatobiliary complications of hematopoietic cell transplantation, 40 years on. *Hepatology*. 2010;51:1450–1460.

16. Hessen M, Akpek EK. Ocular graft-versus-host disease. *Curr Opin Allerg Clin Immunol*. 2012;12:540–547.
17. Lockridge JL, Chen X, Zhou Y, et al. Analysis of the CD1 antigen presenting system in humanized SCID mice. *PLoS ONE*. 2011;6:e21701.
18. Rajesh D, Zhou Y, Jankowska-Gan E, et al. Th1 and Th17 immuno-competence in humanized NOD/SCID/IL2rgammanull mice. *Hum Immunol*. 2010;71:551–559.
19. Atkinson K, Incefy GS, Storb R, et al. Low serum thymic hormone levels in patients with chronic graft-versus-host disease. *Blood*. 1982;59:1073–1077.
20. Fallen PR, McGreavey L, Madrigal JA, et al. Factors affecting reconstitution of the T cell compartment in allogeneic haematopoietic cell transplant recipients. *Bone Marrow Transplant*. 2003;32:1001–1014.
21. Weinberg K, Blazar BR, Wagner JE, et al. Factors affecting thymic function after allogeneic hematopoietic stem cell transplantation. *Blood*. 2001;97:1458–1466.
22. Onoe T, Kalscheuer H, Danzl N, et al. Human natural regulatory T cell development, suppressive function, and postthymic maturation in a humanized mouse model. *J Immunol*. 2011;187:3895–3903.
23. Duan K, Zhang B, Zhang W, et al. Efficient peripheral construction of functional human regulatory CD4(+)CD25(high)Foxp3(+) T cells in NOD/SCID mice grafted with fetal human thymus/liver tissues and CD34(+) cells. *Transplant Immunol*. 2011;25:173–179.
24. Li Q, Zhai Z, Xu X, et al. Decrease of CD4(+)CD25(+) regulatory T cells and TGF-beta at early immune reconstitution is associated to the onset and severity of graft-versus-host disease following allo-geneic haematogenesis stem cell transplantation. *Leuk Res*. 2010;34:1158–1168.
25. Srinivasan M, Flynn R, Price A, et al. Donor B-cell alloantibody deposition and germinal center formation are required for the development of murine chronic GVHD and bronchiolitis obliterans. *Blood*. 2012;119:1570–1580.